

PNE CODA ATTENUATION AND SCATTERING PARAMETERS IN NORTHERN EURASIA

Igor B. Morozov

University of Saskatchewan

Sponsored by National Nuclear Security Administration

Contract No. DE-FC52-05NA26609

Proposal No. BAA05-52

ABSTRACT

Magnitude-yield calibration of Northern Eurasia can be improved by using the large chemical and Peaceful Nuclear Explosion (PNEs) seismic datasets acquired by the Soviet Deep Seismic Sounding (DSS) program. Currently, we are using inversion and numerical modeling to analyze the coda amplitude parameters and P -wave travel times from numerous DSS explosions, which would lead to a detailed empirical mapping of seismic properties within northern Eurasia.

In this report, PNE Lg coda amplitudes from seven profiles are inverted to produce maps of the following new coda parameters: 1) frequency-dependent scattering intensities, 2) geometrical parameter (γ), and 3) effective quality (Q_e). The γ and frequency-independent Q_e parameters replace the traditional frequency-dependent $Q(f) = Q_0(f/f_0)^\eta$ parameterization and provide stability, independence of assumptions of a background model, and convenience in interpretation. As we have shown before, parameter γ also yields itself to independent numerical waveform modeling, correlates with crustal tectonic types, and may be a portable attribute valuable for coda regionalization. All three maps show notable correlations with regional tectonics and with recently derived maps of phase amplitude ratios and Lg Q .

Report Documentation Page				Form Approved OMB No. 0704-0188	
Public reporting burden for the collection of information is estimated to average 1 hour per response, including the time for reviewing instructions, searching existing data sources, gathering and maintaining the data needed, and completing and reviewing the collection of information. Send comments regarding this burden estimate or any other aspect of this collection of information, including suggestions for reducing this burden, to Washington Headquarters Services, Directorate for Information Operations and Reports, 1215 Jefferson Davis Highway, Suite 1204, Arlington VA 22202-4302. Respondents should be aware that notwithstanding any other provision of law, no person shall be subject to a penalty for failing to comply with a collection of information if it does not display a currently valid OMB control number.					
1. REPORT DATE SEP 2008		2. REPORT TYPE		3. DATES COVERED 00-00-2008 to 00-00-2008	
4. TITLE AND SUBTITLE PNE Coda Attenuation and Scattering Parameters in Northern Eurasia				5a. CONTRACT NUMBER	
				5b. GRANT NUMBER	
				5c. PROGRAM ELEMENT NUMBER	
6. AUTHOR(S)				5d. PROJECT NUMBER	
				5e. TASK NUMBER	
				5f. WORK UNIT NUMBER	
7. PERFORMING ORGANIZATION NAME(S) AND ADDRESS(ES) University of Saskatchewan, Saskatoon, Saskatchewan, Canada,				8. PERFORMING ORGANIZATION REPORT NUMBER	
9. SPONSORING/MONITORING AGENCY NAME(S) AND ADDRESS(ES)				10. SPONSOR/MONITOR'S ACRONYM(S)	
				11. SPONSOR/MONITOR'S REPORT NUMBER(S)	
12. DISTRIBUTION/AVAILABILITY STATEMENT Approved for public release; distribution unlimited					
13. SUPPLEMENTARY NOTES Proceedings of the 30th Monitoring Research Review: Ground-Based Nuclear Explosion? Monitoring? Technologies, 23-25 Sep 2008, Portsmouth, VA sponsored by the National Nuclear Security Administration (NNSA) and the Air Force Research Laboratory (AFRL)					
14. ABSTRACT see report					
15. SUBJECT TERMS					
16. SECURITY CLASSIFICATION OF:			17. LIMITATION OF ABSTRACT Same as Report (SAR)	18. NUMBER OF PAGES 11	19a. NAME OF RESPONSIBLE PERSON
a. REPORT unclassified	b. ABSTRACT unclassified	c. THIS PAGE unclassified			

OBJECTIVES

The correct and transportable measurement of attenuation parameters is critical in coda magnitude studies. Recently (Morozov et al., in press) we showed that short-period coda attenuation of regional arrivals can be interpreted in terms of the geometrical spreading (γ) and effective attenuation (Q_e) parameters. Taken together, they represent the generalized attenuation coefficient: $\alpha(f) = \gamma + \pi f / Q_e$. This model removes the commonly observed ambiguity of the frequency-dependent $Q(f)$, and parameter γ becomes most useful for interpretation. Modeling of P -wave coda at regional distances and analysis of two Peaceful Nuclear Explosions in Russia in terms of this concept showed a remarkable agreement, particularly in the values of γ .

In this report, we apply the same parameterization to the inversion of spatially-variable surface-consistent Lg coda parameter $\alpha(f)$ from five PNE profiles in Siberia. Minimalistic model parameterization and the Constrained Simultaneous Iterative Reconstruction Technique (SIRT) are used for unbiased inversion. The resulting map of the geometrical parameter (γ) is in excellent agreement with both modeling and inversion in Morozov et al. (in press). The values of γ differentiate between the crustal tectonic types within the study area and are also in agreement with a summary of over forty worldwide studies (Morozov, in press). In addition, scattering amplitudes are found to be highly variable and strongly correlate with geological structures. Coda Q_e^{-1} values also show pronounced correlations with geological structures, although these values may also be somewhat overestimated compared to two detailed PNE point studies by Morozov et al. (in press).

RESEARCH ACCOMPLISHED

Rationale

Geophysical characterization of the Earth's lithosphere broadly consists of descriptions of its velocity, density, and attenuation structures. Combinations of these parameters are used in a broad range of applications, from providing structural and rheological constraints for geodynamics to event location, discrimination of seismic events, calibration and regionalization. For the first two of these parameters, a variety of precise methods have been developed, but *in situ* attenuation remains notoriously difficult to measure and interpret. In particular, while quality parameter (Q) often showing strong frequency dependence, characterization of such frequency-dependent attenuation ($Q(f)$) may be ambiguous and dependent on model assumptions and inversion methods.

Morozov (in press) recently proposed a new technique for measuring attenuation without the use of the ambiguous $Q(f)$ and illustrated it on a number of examples. In this study, we employ this method to invert coda Q values from five Peaceful Nuclear Explosion (PNE) profiles in Russia and to map the frequency-dependent attenuation across a broad area of Siberia (Figure 1).

Different types of attenuation (body, surface, Lg , and coda waves) are often presented in the following power-law form of frequency-dependence:

$$Q(f) = Q_0 \left(\frac{f}{f_0} \right)^\eta, \quad (1)$$

where Q is the apparent quality parameter, and f_0 is some reference frequency often taken to equal 1 Hz (Aki, 1980). However, as argued by Morozov (in press) and Morozov et al. (in press), parameters of such a power-law dependence may be strongly influenced by the observation process, and in particular by the assumptions made about the geometrical spreading of scattered (in the case of coda Q) or other waves. Parameters Q_0 and η trade off with each other through the uncertainty of the assumed geometrical spreading. The geometrical spreading (GS), in its turn, cannot be considered constant within large areas, and ~10% uncertainties in it can account for much of the observed frequency dependence of the apparent Q (Morozov, in press). Unconstrained variations of GS also make it difficult to correlate attenuation parameters from different regions, and also to link them to lithospheric properties. In seismic calibration and nuclear test monitoring studies, uncertainties in Q_0 , η , and geometrical spreading are particularly undesirable, because they prevent the construction of consistent, seamless models of large areas, and complicate magnitude calibration.

Numerical waveform coda modeling (Morozov et al., in press) showed that for a layered 1-D model with a constant, frequency-independent crustal attenuation, the observed coda $Q(f)$ exhibited a strong dependence on frequency. Although such dependence is often observed in coda Q and Lg Q data (e.g., Der et al., 1986; Campillo, 1987, 1990; Frankel, 1990; Mitchell and Cong, 1998; Benz et al., 1997; Mitchell et al., 1997; McNamara et al. 1996; McNamara, 2000; and Erickson et al., 2005), this modeling shows that it may relate to the crustal structure (particularly to layering) and not necessarily to its rheology, fracturing, or fluid content. Similar observations were made earlier by Anderson et al. (1965) for long-period surface waves and by Mitchell (1991) for Lg waves in the Basin and Range. Strictly speaking, because the values of Q and η trade off with the imprecisely known velocity/density structures, these parameters are not necessarily be associated with attenuation properties and may not reliably correlate with geological structures or with the variations of the physical state of the lithosphere. However, the potential association of the widespread observations of frequency-dependent $Q(f)$ with variations of the structure still has not been examined, and values of Q are typically interpreted as related to rheology, physical state, or fluid content of the lithosphere (e.g., Mitchell et al., 1997).

In the practice of $Q(f)$ interpretations, and in particular in Lg coda Q studies (such as coda magnitude calibration), the sensitivity of coda Q to the frequency is usually overcome by referencing the coda $Q(f)$ dependence to some common frequency level, such as 1 Hz, in all comparisons (e.g., Mitchell et al. 1997; Phillips et al., 2004). However, this still does not resolve the problem of $Q(f)$ ambiguity, as such referencing process depends on the velocity structure through parameter η , making the resulting values less portable. Note that because of the inherent dependence of the results on unconstrained GS, changes in inversion approaches sometimes also lead to updated values of Q_0 and η (for example, indicated by Xie et al. (2006) in relation to Mitchell et al. (1997) or Xie (2002) in relation to McNamara et al., (1996)). Thus, the interplay of the assumed forms of GS and power-law $Q(f)$ in dependence (1) creates a difficult environment for measurements and interpretation of attenuation.

In many coda Q and Lg $Q(f)$, and particularly in nuclear test monitoring studies, Q is treated as a sort of coda-shape or spectral-amplitude shape parameter. When used strictly for matching the observed time-frequency dependent amplitudes, the above model works even with imprecise or even arbitrary GS. However, the ability of matching the amplitudes still does not prove that the propagation model is correct and can be used to constrain the crustal and mantle properties. This problem is well-known in the inversion theory – under-constrained (or over-parameterized) models tend to fit the data perfectly while leaving ambiguities in the solution (Menke, 1989). When interpreting such solutions and comparing them to each other, it is important to avoid using parameter combinations that are related to the unconstrained degrees of freedom. Unfortunately, both Q_0 and η in eq. (1) are such parameters, which co-vary with the unconstrained GS.

To resolve this difficulty of intermixed GS and attenuation effects and the resulting apparent character of $Q(f)$, we proposed (Morozov, in press, and Morozov et al., in press) to incorporate a geometrical spreading parameter γ in the following equation for coda amplitude decay:

$$A(t, f) = A_0(f) t^{-\nu} e^{-\alpha(f)t} = A_0(f) t^{-\nu} e^{-(\gamma + \kappa f)t}, \quad (2)$$

where $\kappa = \pi/Q_0$, and ν is the theoretical GS exponent corresponding to the type of scattered wave modes that is considered as predominant. Arguments for form (2) based on the scattering theory were given by Morozov

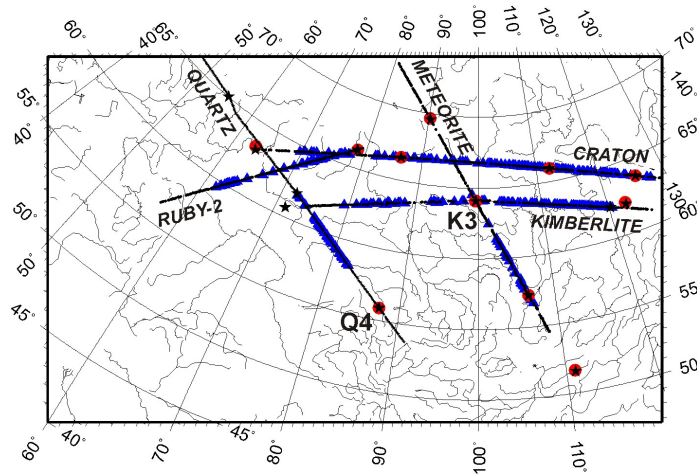


Figure 1. Sources (red circles) and receivers (blue triangles) with measured frequency-dependent coda $d\ln(\text{Amplitude})/dt$ derivatives. Black stars are the PNEs, and small black triangles – 3-component receiver locations. Only 3° grid cells containing sources or receivers were used in the inversion. Two PNEs used in Part I are indicated: Q4 - Quartz-4, and K3 – Kimberlite-3 (see also Figure 2).

(unpublished); however, this expression can also be viewed as a purely empirical approximation (Morozov et al., 2006; Morozov, in press). The subscript “e” in Q_e indicates the “effective” character of the quality parameter, in which we do not differentiate between the intrinsic attenuation and small-scale (Rayleigh- and Mie-type) scattering. Note that parameter κ , and consequently also Q_e , can be frequency-dependent. However, no indications of such dependence were found in several published examples of Lg , and body-wave data (Morozov, in press), and also in surface-wave and normal-oscillation data (Morozov, unpublished).

In parameterization (2), the two parameters (Q_0 , η) of the power law (1) are replaced with three: ν , γ and κ . Within the typical errors of spectral observations, there is little room for seeking frequency-dependent γ or κ , and they can therefore be considered frequency-independent. Morozov (in press and unpublished) re-examined several surface-, body-, Lg -, and coda-wave studies and showed that model (2) was invariably applicable to all of them. In most cases, this resulted in significant increases of the reported values of Q .

Parameter ν significantly trades off with γ , and therefore it is acceptable to use amplitudes $A(t, f)$ corrected for geometrical spreading with fixed ν values determined from theoretical considerations, as it is commonly done in $Q(f)$ studies. In such cases, parameter γ describes the spatial variations of uncompensated geometrical spreading. In the case of regional Lg coda Q of this study, we use a model of cylindrically-propagating coda waves generated within the near-surface. In this case, the spreading area of scattering surrounding the source and/or receiver compensates the geometrical spreading of coda waves, and ν can be set equal to 0 (Morozov and Smithson, 2000). However, this is only a simplified model, and, for example, diving and reflected scattered waves, deeper, or multiple scattering would change the $t^\nu \approx 1$ law, and make it regionally variable. Our objective in this study is to measure these variations, in the form of a spatially-variant γ .

Parameter γ was found to correlate with lithospheric types and ages; in particular, the value of $\gamma_D = 0.008 \text{ s}^{-1}$ appeared to clearly separate the tectonically stable ($\gamma < \gamma_D$) and active areas ($\gamma > \gamma_D$; Morozov, in press). In addition, numerical modeling of the regional P -wave coda conducted in several PNE-based models (Morozov et al., in press) showed that the modeled γ was in a close agreement with the measurements from PNE data, and coda Q could be related to the S -wave crustal Q_S . Therefore, it is particularly interesting to look for correlations of γ with geological structures across a large contiguous area like the PNE profiling area of this study.

From the viewpoint of the classical scattering theory (e.g., Chernov, 1960, p.53; Nikolayev, 1968), parameterization (2) is merely a return to the traditional frequency-dependent attenuation coefficient $\alpha(f)$ instead of the “scattering quality” parameter Q , introduced by Aki (1980). Dainty (1981) gave a justification for expression (2) as describing scattering of 1-30-Hz S -wave on larger scatterers. In coda Q studies, such scattering could occur by means of diving, reflected, and mode-converted waves propagating through the crust. Note that such processes mostly involve deterministic effects, such as ray bending in crustal velocity gradients and reflections from major lithospheric structural contrasts, and therefore the use of Q , leads to undesirable connotation of random scattering and loss of correlation with the structure. Therefore, instead of using Q , we prefer using the uncompensated GS, which simply represents the frequency-independent part of the attenuation coefficient: $\gamma = \alpha(f=0)$.

Preliminary analysis of two PNEs (Figure 1; Morozov et al., in press) suggested that γ values could be remarkably stable, even in the case of surprisingly strong frequency dependence ($\eta \approx 1$) within the Siberian Craton. The observed values of γ also agreed well with those derived from waveform synthetics computed for the study area. We argued that γ could potentially provide a stable and transportable criterion for correlating the observations of attenuation with crustal tectonic types.

In this paper, we further apply the approach arising from parameterization (2) to mapping the short-period attenuation structure in central Siberia by using several PNE datasets (Figure 1). Detailed descriptions of the PNE profiles and geological setting of the study area were recently given by Li et al. (2007 and submitted to BSSA) and are not repeated here. The resulting γ and Q_e maps show good stability and correlations with velocity structures and tectonics. Because the parameters being mapped are directly related to crustal and upper mantle properties, they should also provide a good basis for comparisons to other studies and for incorporation into forward modeling.

Data

The dataset consists of log-amplitude coda amplitude readings from the PNE explosion records from five Deep Seismic Sounding profiles in Russia (Figure 1). Figure 2 shows an example of transverse-component (relative to the

source-receiver direction) record from PNE Kimberlite-3 (labeled K3 in Figure 1) located near the edge of the Siberian Craton. Note the high density of recordings (10–15 km spacing) and the differences in the wavefield propagating within and beneath the West Siberian Basin (west of the PNE) and the Siberian Craton (Figure 2). This PNE was also used in detailed studies by Morozov et al. (in press).

The data were carefully edited by removing poor and clipped records, and all regional arrivals were identified and picked. The *Lg* distance ranges and time windows were selected interactively from all PNE record sections. Coda windows started 20 sec after the picked *Lg* onsets and extended for 50 – 100 sec. Pre-*Lg* noise windows (i.e., the *P*- and *S*-wave coda; cf. Morozov and Smithson, 2000) were also picked. By using these windows, *Lg* to pre-*Lg* amplitude ratios were calculated, and traces with these ratios below 1.1 were discarded.

Edited records were further band-pass filtered within four overlapping frequency bands of 1–2, 1.5–3, 2–4, and 3–5 Hz. Within each band, three-component trace envelopes were formed, and $d\ln(\text{Amplitude})/dt$ derivatives and their standard error estimates were measured by using the “robust fit” technique in Matlab. The resulting values of frequency-dependent log-amplitude coda slopes were saved in a database which was used in the subsequent analysis.

Surface-Consistent (λ, γ, Q_e) Inversion Method

The power and utility of the $\alpha(f)$ model is in its direct link to the observations (Morozov, in press). In the case of regional coda attenuation, coda $\alpha_c(f)$ simply becomes the negative time derivative of the logarithm of coda amplitude (2):

$$\alpha_c(f) = -\frac{d \ln A(t, f)}{dt}, \quad (3)$$

which can be measured by fitting the coda envelopes in each individual record. Because of the source-receiver reciprocity, the observed coda amplitude (2), and consequently $\alpha_c(f)$, contain contributions from scattering near the source and receiver. Spatial separation of these two areas and the corresponding differences in their $\alpha(f)$ values could be significant for mapping, particularly in the case of the long-range PNE sources. Thus, we need to invert the observed $\alpha_c(f)$ for spatial variations in $\alpha(f)$. To accomplish this, we use the surface-consistent approach, and represented $\alpha(f)$ as functions of the coordinates and frequency. The surface-consistent model implies that for the collocated source and receiver, the values of $\alpha(f)$ should be the same, and for spatially close locations, $\alpha(f)$ values are close.

To derive a model for the observed γ and Q_e , we use an approximation for the event-energy envelope by Morozov and Smithson (2000), in which the intensity (energy density) of the primary event was described by a short pulse of parabolic shape arriving at time t_0 , with amplitude P_0 and duration τ . The coda of this arrival was described by exponentially decaying amplitude following the pulse:

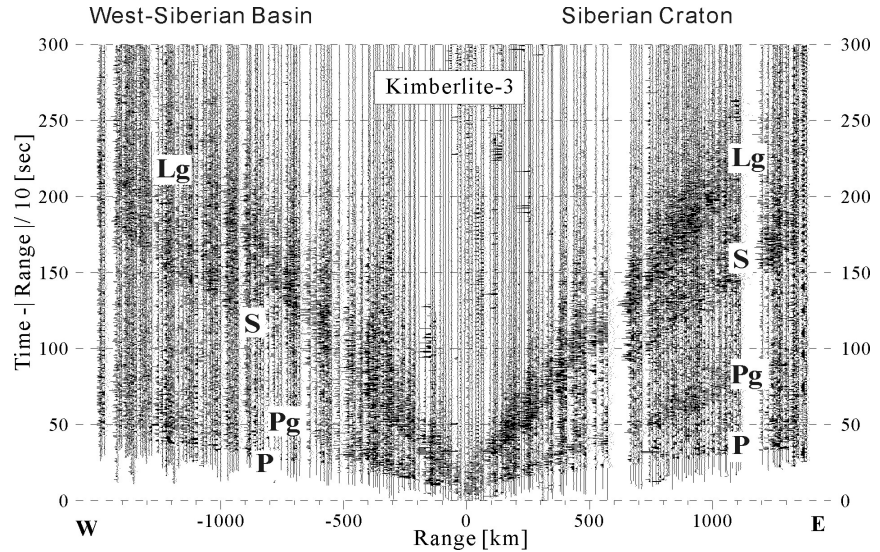


Figure 2. Transverse-component record from PNE Kimberlite-3 (K3 in Figure 1), filtered within 0.5 - 8.0 Hz pass-band. The regional phases (labeled *P*, *Pg*, *S*, and *Lg*) are clear and observed to far source-receiver distances. Note the difference between the branches of *Lg* in two directions from the PNE.

$$P_{\text{coda}}(t, \lambda, \alpha) = \begin{cases} 0, & t < t_0, \\ \lambda(f)P_0 \tau e^{-2\pi f(t-t_0)/Q} = \lambda(f)P_0 \tau e^{-2\alpha(f)t}, & t \geq t_0, \end{cases} \quad (4)$$

where $\lambda(f)$ is the scattering efficiency factor (the relative coda intensity at the time of the primary event). In general, this parameter may also depend on the frequency.

From PNE Quartz-4 records (Q4 in Figure 1), the duration of the primary onsets was estimated as $\tau = 1.25$ s for the teleseismic P , and $\lambda = 0.22$ for all events (Morozov and Smithson, 2000). The relative coda intensity at the time of the primary event was $\lambda\tau \approx 0.27$ (Equation [4]), which can be considered as significantly smaller than 1. Therefore, the total wavefield intensity at the receiver:

$$P_{SR}(t) = [P_{\text{primary}}(t) + P_{\text{coda}}(t, \lambda_S, \alpha_S)] * [P_{\text{primary}}(t) + P_{\text{coda}}(t, \lambda_R, \alpha_R)], \quad (5)$$

(quantities with subscripts S and R correspond to the source and receiver locations, respectively, and the asterisk denotes time convolution) can be approximated to the first order in λ :

$$P_{SR}(t) = P_{\text{primary}}(t) * P_{\text{primary}}(t) + P_{\text{primary}}(t) * [P_{\text{coda}}(t, \lambda_S, \alpha_S) + P_{\text{coda}}(t, \lambda_R, \alpha_R)]. \quad (6)$$

The resulting coda intensity is given by the second term in this expression:

$$P_{SR,\text{coda}}(t) \propto \lambda(x_S, y_S, f) e^{-2\alpha(x_S, y_S, f)t} + \lambda(x_R, y_R, f) e^{-2\alpha(x_R, y_R, f)t}, \quad (7)$$

where we also assumed surface consistency of λ . From eq. (2), $\alpha(x, y, f)$ is further approximated by a linear function of frequency:

$$\alpha(x, y, f) = \gamma(x, y) + \kappa(x, y)f, \quad (8)$$

Taking into account the source and receiver site effects, the coda intensity (7) is further approximated as:

$$P_{SR,\text{coda}}(t) \approx \zeta(f) e^{-2\alpha_c t}, \quad (9)$$

where $\zeta(f)$ is a time-independent amplitude normalization factor of the specific seismic record. With these approximations, eq. (9) leads to the following system of non-linear equations:

$$d_{n,t,f} = \lambda_S(f) e^{-2[\alpha(x_S, y_S, f) - \alpha_c]t} + \lambda_R(f) e^{-2[\alpha(x_R, y_R, f) - \alpha_c]t} - \zeta_n(f) = 0 \quad (10)$$

for all t, f , and record numbers n . Solving equations (10) is equivalent to minimizing the following objective function:

$$\Phi(\gamma, \kappa, \lambda, \zeta) = \frac{1}{2} \sum_f \sum_n \int_{T_n} [\lambda_S(f) e^{-2[\alpha(x_S, y_S, f) - \alpha_c]t} + \lambda_R(f) e^{-2[\alpha(x_R, y_R, f) - \alpha_c]t} - \zeta_n(f)]^2 dt, \quad (11)$$

where T_n is the coda observation time window. The summation in eq. (11) takes place over all records and frequencies of interest, and the minimization is performed in terms of parameters γ , κ , $\lambda(f)$, and $\zeta(f)$. In this study, to improve the stability of the inverse, we did not consider the dependence of κ , λ , and ζ on frequency, and solved for variations of γ , κ , and λ as functions of spatial coordinates only.

To define the spatial inversion grid for parameters γ , κ , and λ , care needs to be exercised in order to not over-parameterize the model excessively. To achieve a “minimalistic” parameterization, we defined a spatial grid with increments of 3° in both latitudes and longitudes covering the entire area of profiling. Only cells containing the actual source or receiver points (Figure 1) were included in the inversion, which resulted in 53 cells. For each of these selected grid cells, a bilinear basis function (finite element) $\psi_i(x, y)$ was defined (x was the longitude, y is the latitude, and i is the cell number), such that $\psi_i(x, y) = 1$ in its center and $\psi_i(x, y) = 0$ at the centers of all other cells.

“Blocky” basis functions typical in travel-time tomography (with $\psi_i(x,y) = 1$ within the entire cell) were also tried, with no significant differences in the results.

With properly defined basis functions, the following identity holds at any point (x, y) :

$$\sum_i \psi_i(x, y) = 1, \quad (12)$$

where the summation includes all cells. With the help of this functional basis, values of γ , κ , and λ at any point (x, y) can be expressed through the corresponding values $(\gamma_i, \kappa_i, \lambda_i)$ at the nodes; for example, for γ :

$$\gamma(x, y) = \sum_i \psi_i(x, y) \gamma_i. \quad (13)$$

Within the class of functions given by the finite-element functional basis (13), the objective function (11) becomes a non-linear function of model parameters: $\Phi(\gamma_i, \kappa_i, \lambda_i, \zeta_n)$. However, unconstrained degrees of freedom are still present in this parameter space, such as an arbitrary scaling of parameters λ and ζ in eq. (11) and source-receiver trade-off caused by non-uniform sampling of the model. These degrees of freedom are typically removed by regularization, which is performed by adding constraint terms to the objective function (11), for example:

$$\tilde{\Phi}(\gamma_i, \kappa_i, \lambda_i, \zeta_n) = \Phi(\gamma_i, \kappa_i, \lambda_i, \zeta_n) + \sum_k w_k \Psi_k(\gamma_i, \kappa_i, \lambda_i), \quad (14)$$

where functions $\Psi_k(\gamma_i, \kappa_i, \lambda_i)$ penalize various undesirable types of instabilities. However, this method of regularization requires a non-trivial selection of weights w_k and biases the solution from minimizing the objective function (11) and satisfying equations (10). Most importantly, properties of the resulting constraints may be difficult to assess in order to evaluate their effects on the interpretation. Therefore, a simpler regularization scheme with readily interpretable constraints would be preferable.

In order to obtain a stable solution without being unbiased from the minimum of $\Phi(\gamma_i, \kappa_i, \lambda_i, \zeta_n)$, we utilized the iterative nature of the SIRT (Simultaneous Iterative Reconstruction Technique) solver that we employed. After each iteration, the solution was corrected to satisfy the following criteria:

- 1) $\lambda_i \geq 0$ and $\kappa_i \geq 0$ at all points. These constraints correspond to non-negative scattering amplitude and Q , respectively. Note that unlike κ_i , γ_i can take both negative and positive values.
- 2) $\sum_i \lambda_i = N_{\text{grid}}$, where N_{grid} is the total number of grid points involved in the inversion. This constraint was enforced by rescaling all values of λ_i and removing the scaling invariance of the minimum of expression (11).
- 3) $|\lambda_i - \lambda_i^{\text{smooth}}| < \beta \lambda_i^{\text{smooth}}$, where $\lambda_i^{\text{smooth}}$ is the smoothed value of λ_i derived by averaging the adjacent points (and excluding the i -th one), and β is the tolerance parameter selected equal to 0.05 in our inversion. This criterion guaranteed that adjacent cells differ by no more than β in terms of λ_i . Similar constraints were implemented for γ_i and κ_i .
- 4) Additionally, similar constraints, for example: $|\lambda_i - \lambda_i^{\text{apriori}}(x, y)| < \beta' \lambda_i^{\text{apriori}}(x, y)$, could be added to keep the solution in the vicinity of some *a priori* model. Such constraints could be useful to remove instabilities at isolated points near the circumference of the model, or for extrapolation of the solution outside of the area of coverage. The *a priori* model can be parameterized at user-specified sets of support points between which the values of $\lambda^{\text{apriori}}(x, y)$ are linearly interpolated by using a Delaunay triangulation. However, we did not use such constraints in the solution presented below.

To invert for γ_i , κ_i , λ_i , and ζ_n numerically, we used the SIRT method by applying it directly to Equation 10. For a small parameter perturbation, these equations become:

$$d_{f,n,t} = d_{f,n,t}^0 + \delta d_{f,n,t} = d_{f,n,t}^0 + [\delta \lambda_s - 2t(\delta \gamma_s + f \delta \kappa_s)] e^{-2(\alpha_s - \alpha_c)t} + [\delta \lambda_R - 2t(\delta \gamma_R + f \delta \kappa_R)] e^{-2(\alpha_R - \alpha_c)t} - \delta \zeta_n = 0. \quad (15)$$

Quantities $\delta\gamma$, $\delta\kappa$, and $\delta\lambda$ evaluated at the source and receiver locations are further expressed as combinations of the corresponding values at the nearest grid nodes by using equation 13. By combining all parameter perturbations $\delta\gamma_i$, $\delta\kappa_i$, $\delta\lambda_i$, and $\delta\zeta_n$ into one model vector \mathbf{p} , the resulting equations form a linear system:

$$\mathbf{A}\delta\mathbf{p} - \mathbf{B} = \mathbf{0}, \quad (16)$$

which was over- or mixed-determined (Menke, 1989; 7,986 data points and 885 unknowns in our inversion). Its approximate solution in the least-squares sense is:

$$\delta\mathbf{p} = (\mathbf{A}^T \mathbf{A})^{-1} \mathbf{A}^T \mathbf{B}, \quad (17)$$

where T denotes the matrix transpose. In SIRT (and related back-projection methods), the diagonally-dominant $\mathbf{A}^T \mathbf{A}$ matrix is replaced in this equation with its diagonal, whose inverse can be easily calculated:

$$\delta\mathbf{p} \approx c [\text{diag}(\mathbf{A}^T \mathbf{A})]^{-1} \mathbf{A}^T \mathbf{B}. \quad (18)$$

This method requires the storage of only two vectors: $\mathbf{A}^T \mathbf{B}$ and the diagonal of $\mathbf{A}^T \mathbf{A}$, and consequently it can be efficiently applied to very large problems. In our study, the inverse (18) was calculated during iterative scanning through the entire $s_c(f)$ dataset, and was terminated when model updates became sufficiently small. Between the iterations, “trimming” operations were applied to the model in order to make it satisfy the constraints above. Our final model (Figure 3) resulted in ~90% data error reduction from the starting model with $\gamma_i = 0$, $\kappa_i = 0$, and $\lambda_i = 1$. To suppress parameter oscillations during this process, a scaling factor $c < 1$ ($c = 0.5$ in our inversion) was applied during stepping (18) and was gradually reduced when data error increases were detected.

Results

The resulting maps of λ , γ , and κ within the area of Lg coda Q data coverage from five PNE profiles are shown in Figure 3. To produce continuous maps, we used linear interpolation within a Delaunay triangulation constructed on the centers of the 53 grid cells that were used in the inversion (Figure 1). This explains the shapes of some of the features located near the edges of the coverage area (such as the Baikal Rift zone and the Urals; Figure 3).

As expected, the scattering amplitudes, λ , show strong variations which remarkably well correlate with tectonic areas (Figure 3a). High λ values are found in the Uralian and in the Sayan-Baikal (labeled BR in Figure 3b) fold belts which could potentially be related to stronger surface topography and complex crustal structures due to folding. High scattering amplitudes are also present in the western part of the Siberian Craton. By contrast, the eastern part of the Siberian Craton (the Minusinsk-Aldan High; Figures 3a and b) and most of the West Siberian Basin show low λ .

The geometrical spreading exponent, γ , also correlates with tectonics (Figure 3b). Note that the level of $\gamma_D = 0.008 \text{ s}^{-1}$ (purple color in Figure 3b, marked) separates the stable cratonic areas (with $\gamma < \gamma_D$) from the tectonically active Baikal Rift, for which γ is distinctly higher than γ_D . As Morozov et al. (in press) showed by numerical modeling, such a difference could be caused by generally higher level of contrasts within the tectonically active crust, potentially with presence of relatively thin attenuative zones. As these authors also suggested, within stable parts of the study area, γ varies only moderately, from about 0.004 to 0.007 s^{-1} (Figure 3b).

The effective surface-consistent coda Q_e^{-1} values, defined as $Q_e^{-1} = \kappa/\pi$, also show a distinct correlation with tectonic structures and reasonable stability within the study area (Figure 3c). Coda Q_e is low in the Baikal Rift zone ($Q_e \approx 100$) and near the Urals ($Q_e \approx 130$) but higher within the Siberian Craton ($Q_e \approx 300$). Within the eastern part of the West Siberian Basin, the attenuation is the lowest ($Q_e \approx 1000$). However, although indicating a reasonable correlation with the geological structures, the values of Q_e^{-1} appear somewhat over-estimated (could be to a factor of about 2) compared to detailed measurements performed on two individual PNEs (Morozov et al., in press). Potential reasons for such an overestimation will be considered in future research.

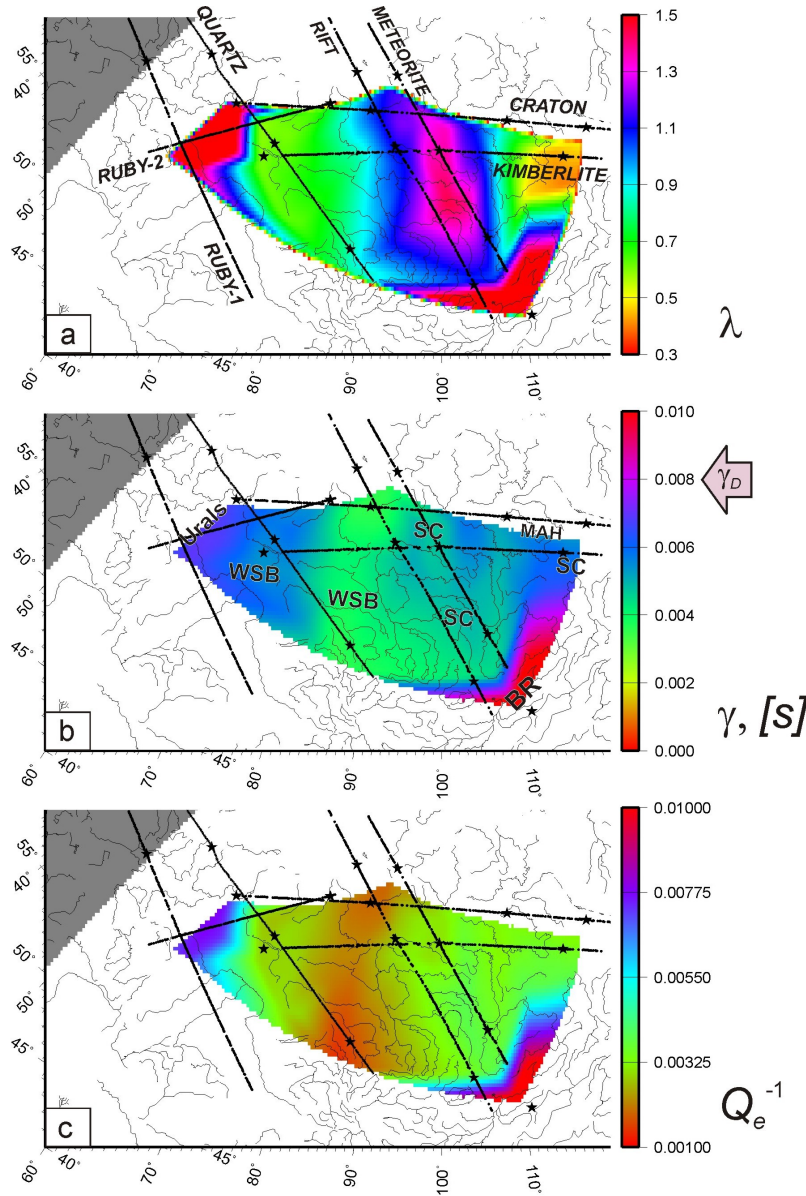


Figure 3. PNE L_g coda Q inversion results: a) coda scattering amplitude λ ; b) uncompensated geometrical spreading γ ; 2) effective coda attenuation $Q_e^{-1} = \kappa/\pi$. In plot b), note the level of $\gamma_D = 0.008 \text{ s}^{-1}$ which was suggested to discriminate between stable and active tectonic areas (Morozov, in press). Major tectonic regions are indicated in plot b): BR – Baikal Rift; SC – Siberian Craton; MAH – Minusinsk-Aldan High; WSB – West Siberian Basin PNE profiles are labeled in plot a).

CONCLUSIONS AND RECOMMENDATIONS

Morozov et al. (in press) demonstrated that short-period coda attenuation of regional arrivals can be interpreted as a combination of uncompensated geometrical spreading (γ) and effective attenuation (Q_e). Taken together, these parameters represent the generalized attenuation coefficient: $\alpha(f) = \gamma + \pi f/Q_e$, which in many cases can be measured directly from the data. Parameter γ removes the common ambiguity of the $Q(f)$ and is most useful for correlating different study areas and tectonic types. Modeling of P -wave coda at regional distances and analysis of two Peaceful Nuclear Explosions in Russia in terms of this concept showed a remarkable agreement, especially in γ values.

In this report, we applied the same parameterization to the inversion of spatially-variable surface-consistent L_g coda parameters from five PNE profiles in Siberia. The resulting map of the geometrical parameter (γ) is in excellent agreement with both modeling and inversion in Part I, and also with a summary of over forty worldwide studies (Morozov, in press). In addition, scattering amplitudes were found to be highly variable and strongly correlate with geological structures. Coda Q_e^{-1} values also showed pronounced correlation with geological structures, although these values also appeared somewhat overestimated compared to the detailed point studies in Morozov et al. (in press).

REFERENCES

- Aki, K. (1980). Scattering and attenuation of shear waves in the lithosphere, *J. Geophys. Res.* 85: 6496–6504.
- Anderson, D. L., A. Ben-Menahem, and C. B. Archambeau (1965). Attenuation of seismic energy in the upper mantle, *J. Geophys. Res.* 70: 1441–1448.
- Benz, H., A. Frankel, and D. Boore (1997). Regional L_g attenuation in the continental United States, *Bull. Seism. Soc. Am.* 87, 600–619.
- Campillo, M. (1987). L_g wave propagation in a laterally varying crust and the distribution of the apparent quality factor in central France, *J. Geophys. Res.* 92: 12604–12614.
- Campillo, M. (1990). Propagation and attenuation characteristics of the crustal phase L_g , *PAGEOPH*, 132, 1–17.
- Chernov, L. A., *Wave Propagation in a Random Medium*, pp. 35–57, McGraw-Hill, New York, 1960.
- Dainty, A. M. (1981). A scattering model to explain seismic Q observations in the lithosphere between 1 and 30 Hz, *Geophys. Res. Lett.* 8: 1126–1128.
- Der, Z. A., A. C. Lees, and V. F. Cormier (1986). Frequency dependence of Q in the mantle underlying the shield region of Eurasia, Part III: The Q -model, *Geophys. J. R. Astr. Soc.* 87: 1103–1112.
- Erickson, D., D. E. McNamara, and H. Benz (2005). Frequency-dependent L_g Q within the continental United States, *Bull. Seism. Soc. Am.* 94: 1630–1643.
- Frankel, A., A. McGarr, J. Bicknell, J. Mori, L. Seeber, and E. Cranswick (1990). Attenuation of high-frequency shear waves in the crust: measurements from New York State, South Africa, and southern California, *J. Geophys. Res.*, 95; 17441–17457.
- McNamara, D. E. (2000). Frequency-dependent L_g attenuation in south-central Alaska, *Geophys. Res. Lett.* 27: 3949–3952.
- McNamara, D. E., T. J. Owens, and W. R. Walter (1996). Propagation characteristics of L_g across the Tibetan Plateau, *Bull. Seism. Soc. Am.* 86: 457–469.
- Menke, W., 1989. Geophysical data analysis: Discrete inverse theory, Academic press, San Diego, CA, p. 35–60.
- Mitchell, B. J. (1991). Frequency dependence of Q_{Lg} and its relation to crustal anelasticity in the Basin and Range Province, *Geophys. Res. Lett.* 18: 621–624.
- Mitchell, B. J., and Cong, L. (1998). L_g coda Q and its relation to the structure and evolution of continents: a global Perspective, *Pure Appl. Geophys.* 153: 655–663.
- Mitchell, B. J., Pan, Y., Xie, J., and Cong, L. (1997). L_g coda Q variation across Eurasia and its relation to crustal evolution, *J. Geophys. Res.* 102: 22767–22779.
- Morozov, I. B. and Smithson, S. B. (2000). Coda of long-range arrivals from nuclear explosions, *BSSA* 90: 929–939.
- Morozov, I. B. (*Geophys. J. Int.*, in press). Geometrical attenuation, frequency dependence of Q , and the absorption band problem, manuscript available at:
http://seisweb.usask.ca/downloads/Papers/Q_2008/Morozov_Qf_GJI_Apr2008.2.pdf

- Morozov, I. B., C. Zhang, J. N. Duenow, E. A. Morozova, and S. Smithson, (*Bull. Seism. Soc. Am.*, *in press*). Frequency dependence of regional coda Q : Part I. Numerical modeling and an example from Peaceful Nuclear Explosions, Manuscript available at:
http://seisweb.usask.ca/downloads/Papers/Coda_Q_Modeling_2007/Morozov_et_al_Coda_Q.2.pdf
- Morozov, I., Morozova, E., Zhang, C. Chubak, G., Phillips, W.S. and Lipovetsky, I. (2006). Magnitude-yield and travel-time calibration of northern Eurasia using deep seismic sounding datasets, in *Proceedings of the 28th Seismic Research Review: Ground-Based Nuclear Explosion Monitoring*, LA-UR-06-5471, Vol. 1, pp. 130–140.
- Nikolayev, A. V. (1968). Seismic properties of weakly heterogeneous media (Engl. Transl.) *Acad. Sci. USSR Phys. Solid Earth*, 83–87.
- Phillips, W.S., H.J. Patton, S.R. Taylor, H.E. Hartse, and R.E. Randall, (2004). Calibration for coda based magnitude and yield, in *Proceedings of the 26th Seismic Research Review: Trends in Nuclear Explosion Monitoring*, LA-UR-04-5801, Vol. 1, pp. 449–456.
- Xie, J. (2002) $L_g Q$ in the eastern Tibetan Plateau, *Bull. Seism. Soc. Am.* 92: 871–876.